AUTOMATIC ECG WAVE EXTRACTION IN LONG-TERM RECORDINGS USING GAUSSIAN MESA FUNCTION MODELS AND NONLINEAR PROBABILITY ESTIMATORS

Rémi Dubois*[,a], Pierre Maison-Blanche [b], Brigitte Quenet [a], Gérard Dreyfus [a]

a) Laboratoire d'Électronique (CNRS UMR 7084),

ESPCI-Paristech, 10 rue Vauquelin 75005 Paris, France

b) Lariboisière hospital, APHP, Paris 7 University, France

Abstract

This paper describes the automatic extraction of the P, Q, R, S and T waves of electrocardiographic recordings (ECGs), through the combined use of a new machine-learning algorithm termed Generalized Orthogonal Forward Regression (GOFR) and of a specific parameterized function termed Gaussian Mesa Function (GMF). GOFR breaks up the heartbeat signal into Gaussian Mesa Functions, in such a way that each wave is modeled by a single GMF; the model thus generated is easily interpretable by the physician. GOFR is an essential ingredient in a global procedure that locates the R wave after some simple pre-processing, extracts the characteristic shape of each heart beat, assigns P, Q, R, S and T labels through automatic classification, discriminates normal beats (NB) from abnormal beats (AB), and extracts features for diagnosis. The efficiency of the detection of the QRS complex, and of the discrimination of NB from AB, is assessed on the MIT and AHA databases; the labeling of the P and T wave is validated on the QTDB database.

Keywords: machine-learning, neural network, orthogonal forward regression, adaptive signal processing, cardiac wave recognition, ECG.

*corresponding author: remi.dubois@espci.fr
Tel: +33 1 40 79 46 96, fax: +33 1 47 07 13 93

I. Introduction

Long-term ECGs have many applications, especially 24 hours records that reflect the effects of daily physical activities. Due to their ambulatory character, such ECGs tend to be very noisy, and often require analysis by experts [1], [2], [3]. Reviewing and editing long-term ECG data are time-consuming processes, although the data stream may contain a very small amount of clinically relevant information. Algorithms have been developed to automatically detect, classify and analyze electrical cardiac complexes [4], [5], [6], [7], [8], [9], [10]: they include wavelet decomposition [11], [12], and radial basis function (RBF) modeling [13]. In addition to these methods for parameter extraction, several automatic classification methods have been used for labeling the cardiac waves such as neural networks [14], [15], Hidden Markov Models [16], [17], [18] or Support Vector Machines [19]. But the specificity and the sensitivity of such algorithms are far from being fully satisfactory. Even for 10-second ECGs obtained in supine conditions, there is still a need for improved solutions [20], [21].

In the present paper, we describe a new algorithm, which automatically detects the electrical waveforms from cardiac complexes (P-Q-R-S-T), and further discriminates abnormal beats (AB) from normal beats (NB) originating from the sinus node. The core of our method is the modeling of cardiac beats by a new class of parameterized functions (Gaussian Mesa Functions or GMFs) which were specially designed for modeling each cardiac waveform by a single function. The estimation of the parameters of the GMF is performed by an original algorithm termed Generalized Orthogonal Forward Regression (GOFR). Once a heartbeat is segmented into GMFs, a medical assignment (P, Q, R, S or T) for each function is performed automatically, based on probability estimations provided by neural networks. The latter step is performed with remarkable accuracy and simplicity, due to the fact that the GMF modeling extracts features that are very relevant for quantitative electrocardiology.

The above algorithms are embedded into a global analysis procedure that does not require any ad-hoc adaptation for a given ECG recording, and allows multi-lead ECG processing: manual lead selection by the cardiologist is not required.

II. Methods

Figure 1 shows pictorially an overview of the whole algorithm described in this section. Although the paper focuses on the second step (heartbeat processing), preprocessing, which is a prerequisite for ECG analysis, is briefly described; examples of post-processing are described for performance assessment.

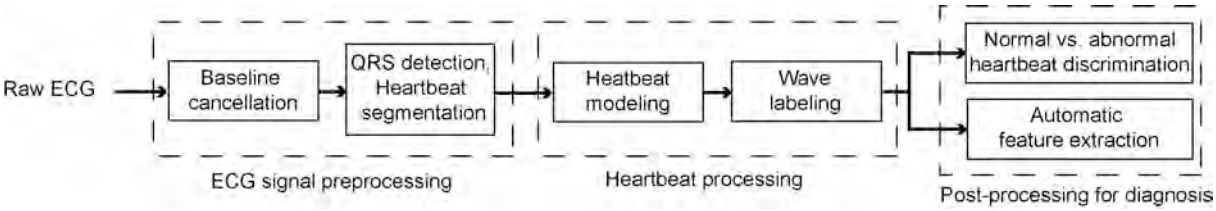

Figure 1

Overview of the global analysis procedure ECG preprocessing

II.1. ECG Signal preprocessing

In this study, the preprocessing methods used are unsophisticated, but they are suitable for the data present in the AHA [22] and MIT [23] databases used here. The first step is the computation of the electrical baseline, in order to obtain an iso-electric reference for the computation of the waveform amplitude. The algorithm that corrects for baseline variations is based on the detection of the active and passive zones of the signal (an active zone is defined as a time interval during which the heart has an activity); the result of that step is a relatively flat iso-electric baseline, together with an estimate of the noise level. The ECG signal is subsequently segmented into cardiac complexes by an efficient and popular algorithm developed by Pan and Tompkins [24].

Since the focus of this paper is the heartbeat processing described in the next section, the baseline correction and the segmentation of the raw signal into heartbeats are not detailed in this paper but are only introduced as a part of the whole procedure for the analysis of the MIT and AHA databases. Interested readers may refer to [25] and [26] for a detailed description; many examples are provided in [25], pages 59 - 64 and 84 - 90.

II.2. Heartbeat processing

In the present approach, heartbeat processing is performed in two steps, namely heartbeat modeling and wave labeling. To model the heartbeat, a new function, called Gaussian Mesa Function (GMF), was introduced; in addition, an original machine learning algorithm, called

Generalized Orthogonal Forward Regression (GOFR), was designed for adapting those functions to the cardiac signal [26], [27]. The purpose of coupling GMF and GOFR is to provide a mathematical model in which each monophasic cardiac waveform from the body surface ECG is modeled by a single GMF, and each biphasic waveform by two GMFs, which greatly facilitates the subsequent labeling of the waves. The GMF function is defined in section II.2.1, and the GOFR algorithm in section II.2.2. The labeling procedure, which performs the labeling of each cardiac wave from the corresponding GMF(s) is described in section II.2.3.

II.2.1. Gaussian Mesa Function (GMF)

The electrical cardiac cycle on surface ECG is typically represented by 3 waveforms: P, QRS and T. Both P and T waves can be monophasic or biphasic, and the QRS complex is composed of up to three monophasic waveforms Q, R and S. A biphasic waveform can be seen as two monophasic waveforms of opposite polarities.

On a given ECG lead, each monophasic cardiac waveform may have a positive or a negative polarity depending on the orientation of the cardiac electrical activity with respect to the derivation under consideration. These individual waves may be flat or tall, narrow or wide, symmetric or asymmetric, or may exhibit a plateau. A Gaussian Mesa function (GMF) is a parameterized function that was designed to model the variability of monophasic waveforms. It is an asymmetric function with five parameters, made of two half-Gaussian functions connected together by a horizontal line (Figure 2). The shape of the GMF depends on its five parameters.

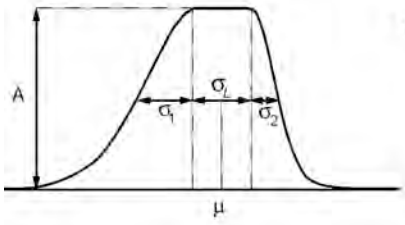

$$B(x,\mu,\sigma_1,\sigma_2,\sigma_L,A) = \begin{cases} A\exp\left(-\frac{1}{2}\left(\frac{x-(\mu-\sigma_L/2)}{\sigma_1}\right)^2\right) & \text{if } x \le \mu-\sigma_L/2 \\ A & \text{if } \mu-\sigma_L/2 \le x \le \mu+\sigma_L/2 \\ A\exp\left(-\frac{1}{2}\left(\frac{x-(\mu+\sigma_L/2)}{\sigma_2}\right)^2\right) & \text{if } x \ge \mu+\sigma_L/2 \end{cases}$$

Figure 2

Definition of the Gaussian Mesa Function

That function is continuous, differentiable, and all its derivatives with respect to its parameters are continuous, which is essential when applying standard optimization algorithms for parameter estimation.

The 5 parameters are thus: μ (location in time), σ_1 (standard deviation of the first Gaussian function), σ_2 (standard deviation of the second Gaussian function), σ_L (length of the horizontal part), A (amplitude of the GMF). The following constraints must be satisfied: σ_1, $\sigma_2 > 0$, $\sigma_L \geq 0$.

II.2.2. Modeling algorithm

In order to efficiently fit parameterized functions to a biological signal, a new algorithm, termed Generalized Orthogonal Forward Regression (or GOFR), was developed. The efficiency of GOFR, as compared to that of the standard OFR (or projection-pursuit) algorithm, was investigated in [26], [27] together with a precise mathematical description. We provide a general description below.

Let s be the signal to be modelled with M GMFs. The GOFR algorithm is a 4-step procedure used to select and tune the parameters of one GMF function. To obtain a model composed of M functions, the four steps of the GOFR are iterated M times.

The 4 steps are the following:

- selection of the most relevant GMF from a library of candidate GMFs,
- tuning of the GMF parameters in order to fit the signal s,
- orthogonalization of the library,
- orthogonalization of s with respect to the tuned GMF.

Since the purpose of the method is to model each of the five characteristic cardiac waveforms with a single GMF, M=6 GMFs were used in this study. Five characteristic waves are modeled by five GMFs out of six, and the sixth GMF either models a non-informative part of the signal, or contributes to the modeling of a biphasic P, R or T wave. The discrimination between informative and non-informative GMFs is performed by the classification procedure described in sections II.2.3.1 and II.2.3.2.

Figure 3 describes the GOFR algorithm. Figure 3A shows the 67 GMFs of the library available at the beginning of the GOFR (M=1, step 1). A correlation coefficient is computed between each GMF of the library and s_1, where s_1 is equal to signal s at the first iteration. The first GMF g_1 selected to model s_1 is the GMF that is most correlated to s_1 (Figure 3B).

The five parameters of g_1 are subsequently tuned to fit s_1. To that end, the BFGS (Broyden-Fletcher-Goldfarb-Shanno) non linear optimisation algorithm [28] minimizes the least squares cost functions (sum of squared differences between s_1 and g_1). Note that constrained optimization is required since σ_1, σ_2 and σ_L must be positive.

The GMF g_1^* obtained after optimisation is shown on Figure 3C.

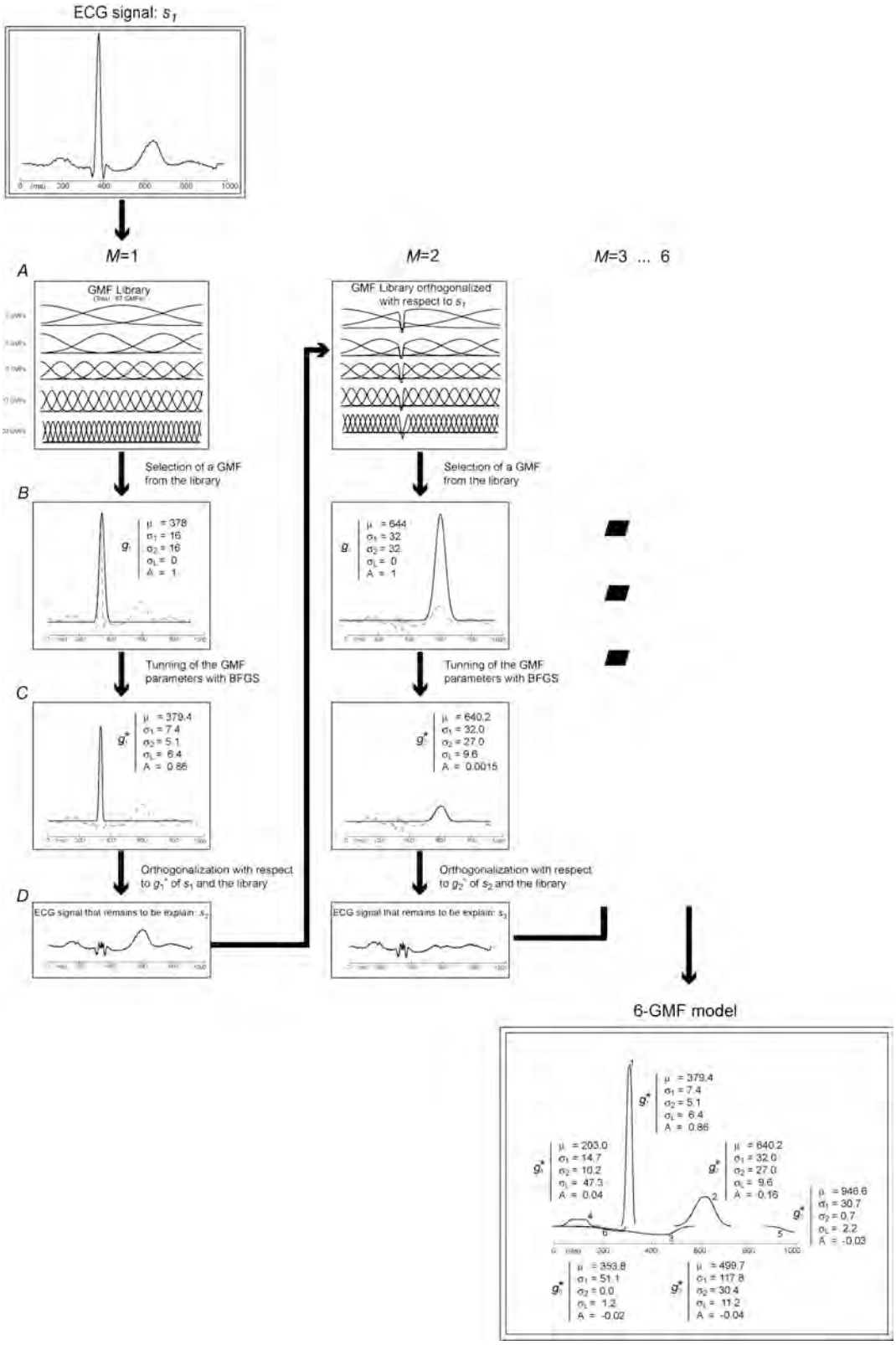

Figure 3

GOFR algorithm for selection, tuning and orthogonalization of a GMF (μ, σ_1, σ_2 and σ_L are in ms; A is in arbitrary units, proportional to the amplitude in mV).

The last two steps consist of orthogonalizing both the library and s_1 with respect to g_1^*. The resulting signal s_2 (Figure 3D) is the part of the ECG that remains to be explained, and is used to iterate the 4 steps described above with the ortogonalized library.
After M=6 iterations, the algorithm provides a model made of 6 GMFs (Figure 3, right panel).

Figure 4 shows representative GMF models for (a) a normal beat, (b) an aberrant beat from the ventricle, (c) a beat with an abnormal ST segment, and (d) a premature beat originating from the atria. Each GMF, selected and tuned by the GOFR algorithm, has an electrophysiological background, and conversely, each monophasic wave is modeled by a single GMF: for example, in Figure 4(a), the first GMF models the signal arising from the repolarization process of the ventricles, GMFs number 2 and 6 refer to ventricle depolarization, and the atria contraction is modeled by GMF number 3. The fourth and the fifth GMFs are not informative, and do not correspond to physiological activity. Note that the specific number attached to each GMF has no significance: the information presented to the physician is not those numbers, but the labels (P, Q, R, S, T) obtained automatically as described in the next section (II.2.3). The advantage of that modeling strategy appears clearly in Figure 4(d): in that case, the GMF that is labeled as a P wave (by the algorithm described in section II.2.3) has negative amplitude, which reflects the fact that the P wave has negative amplitude.
Those four examples are extracted from the MIT and AHA databases, used to validate the modeling algorithm; for more details on those databases, see section III.

II.2.3. GMF labeling

The previous section described the procedure whereby each heartbeat is modeled by six Gaussian Mesa Functions. The next step consists in assigning to each GMF an "electrophysiological" label (P, Q, R, S or T). To perform that task, automatic classifiers are trained to estimate the probability for each GMF to be assigned a given label, from the values of its five parameters defined in section II.2.1.
The task is performed in two steps: first, the R waves are labeled. Then the P, Q, S, and T labels are assigned to the GMFs.

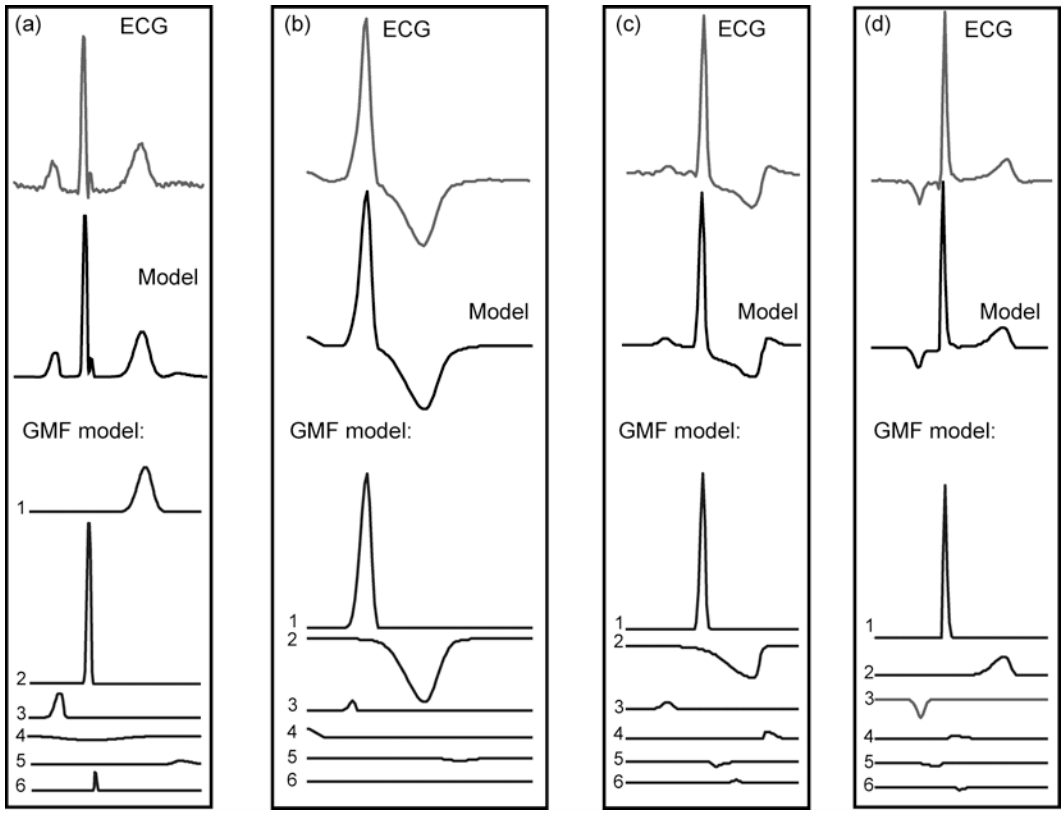

Figure 4

Four heartbeats modeled by six Gaussian mesa functions, fitted with the GOFR algorithm: (a) normal cardiac beat originating from the sinus, (b) abnormal beat of ventricular origin, (c) abnormal ST segment, and (d) premature atrial beat.

II.2.3.1. Labeling of R waves

Among the six GMFs that build up the heartbeat model, the function that models the R wave is first identified. To that end, a neural network classifier (NNC) is trained to estimate the probability of each GMF to model an R wave (Figure 5), in order to discriminate GMFs that model R waves from GMFs that model non-R waves. A cursory introduction to neural network classification is provided in Appendix A.

In the present case, the features that are input to the classifier are the five parameters of the Gaussian mesa function to be labeled: the parameters of the six GMFs that model the heartbeat are input in turn to the classifier, and the GMF that has the highest probability of being a R wave is assigned label “R” (Figure 6). Since the Gaussian mesa function has been specifically designed for fitting a cardiac wave by a single function, the features that are fed to the classifier are very discriminating, thereby facilitating to a great extent the task of the classifier.

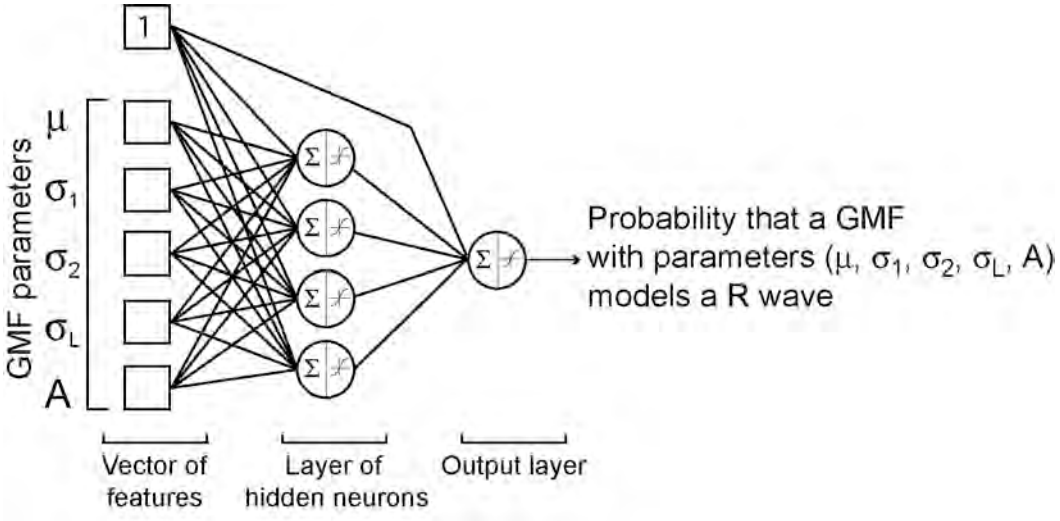

Figure 5

A classifier designed to estimate the probability that a GMF, whose parameters are fed to the classifier, models an R wave.

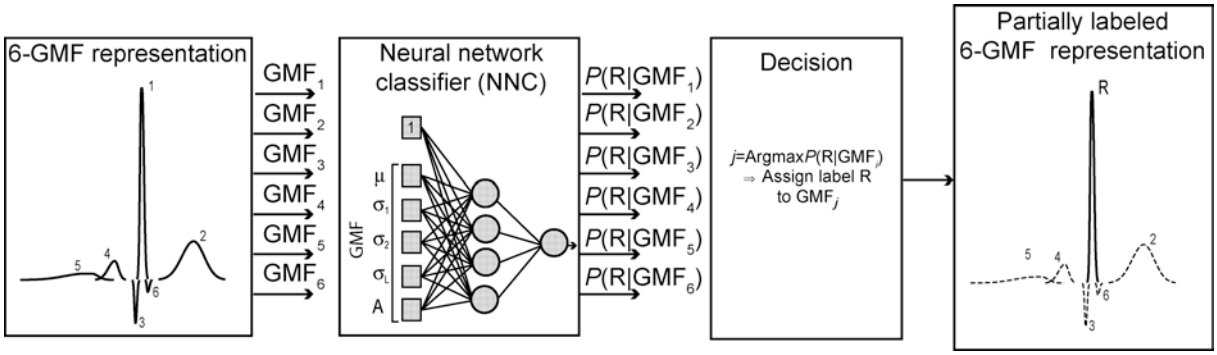

Figure 6

Procedure for assigning label R to one GMF out of a 6-GMF representation of a heartbeat. $P(R|GMF_i)$ denotes the probability for the *i*-th GMF to be an R wave, hence a probability 1 - $P(R|GMF_i)$ of being a non-R wave.

In the usual framework of statistical machine learning, classifiers of increasing complexity are trained on a "training set", and the selection of the optimal complexity (i.e. the number of "hidden" neurons) is performed on a "validation set", which is distinct from the training set. Both data sets are composed of digital ECGs from ELA Medical database on which each cardiac wave has been manually labeled by a cardiologist (P. Maison-Blanche). For R-wave labeling, 960 GMFs that model R waves (R GMFs) and 960 GMFs that do not model R waves (non-R GMFs) are used for training; validation is performed on a different set of 960 R GMFs and 960 non-R GMFs. The results on both data sets, and the selected complexity, are

presented on Table 1 for the R wave classifier, together with the data pertaining to the classifiers of P, Q, S and T, described in the next section.

	Number of hidden neurons selected	Size of the training set	Size of the validation set	Misclassification rate on the training set (%)	Misclassification rate on the validation set (%)
R NNC	4	1920	1920	4	2.7
P NNC	3	1464	1710	0.3	0.5
Q NNC	3	600	290	2.8	2
S NNC	3	956	824	2	1.5
T NNC	5	2238	2506	0.5	0.8

Table 1

Results on the training set and validation set for each classifier; the choice of the decision thresholds used for P, Q, S and T classifiers is explained in the next section

II.2.3.2. Labeling P, Q, S and T waves

Prior to the labeling of P, Q, S and T waves of a given GMF model, a new time origin t_0 is chosen at the location of the R wave previously detected. Therefore the value of the parameter μ of each GMF, which expresses its location, is changed to μ - t_0 (Figure 7); that provides a temporal description of the sequence of activity of the beat, which is important for the labeling process. For example, the new value of μ for the GMF that models a P wave of a normal beat is negative around 120 and 200 ms, so that a GMF with a negative value of μ has a large probability of being a P wave. Conversely, a GMF with μ around 300 ms has a large probability of being a T wave.

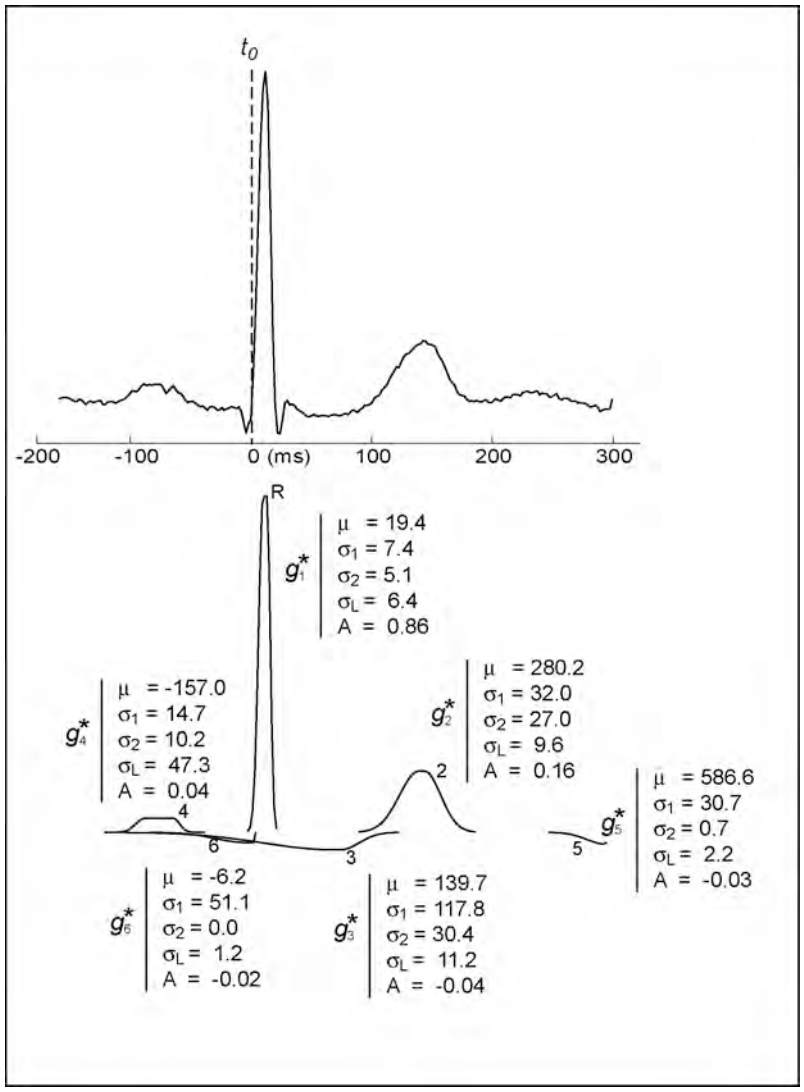

Figure 7

A new time origin t_0 is defined at the bottom of the detected R wave. The value of μ of each GMF of the heartbeat model shown on Figure 3 is changed by $\mu - t_0$ (μ, σ_1, σ_2 and σ_Λ are in ms; A is in arbitrary untis, proportional to the amplitude in mVolts).

Assigning label P

To assign label P to one or more GMF, a neural network classifier (NNC) has been trained to recognize a P-GMF from its parameters. The architecture and the performances of the selected NNC are indicated in Table 1.

Similarly to the assignment of label R, assigning P label to the GMF among the 6 GMFs for which the probability is highest would result in assigning label P once and only once per heartbeat; that procedure would not account for biphasic P modeled by two GMFs to which the same label should be assigned twice. Therefore, a probability threshold must be chosen,

and label P is assigned to all GMFs for which the probability estimated by the NNC is above this threshold (Figure 8).

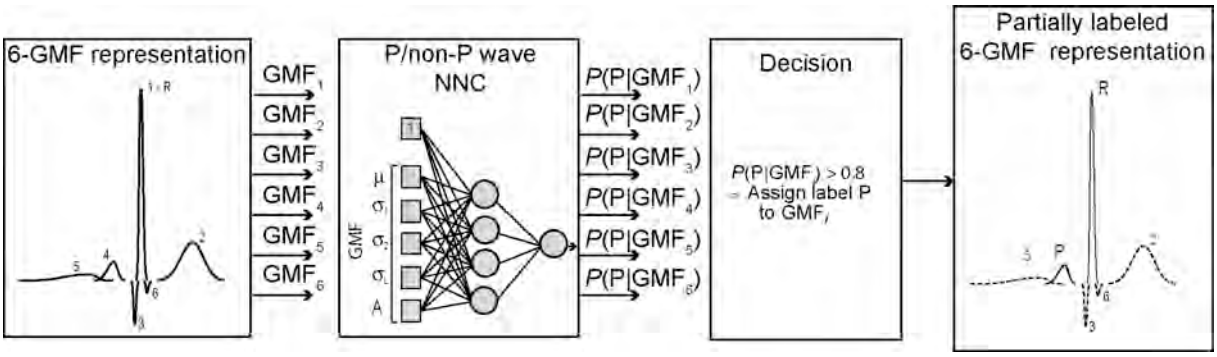

Figure 8

Procedure for assigning label P to one or more GMFs. $P(P|GMF_i)$ denotes the probability for the *i*-th GMF to be a P wave, hence a probability 1 - $P(P|GMF_i)$ of being a non-P wave. The label P is assigned to all GMFs whose probability to be a P wave is higher than 0.8

The choice of the threshold must result in a satisfactory tradeoff between sensitivity and specificity. A graphical representation (ROC – Receiver Operating Characteristics – curve [29]) is used: the true positive rate is plotted against the false positive rate for the different values of the thresholds. Figure 9 shows the ROC curve for the P wave NNC. The area under the curve is larger than 0.9, which provides an estimate of the statistical accuracy of the classifier [29]. For this classifier, choosing a threshold value of 0.8 guarantees high sensitivity with low false positive rate. Increasing the threshold would result in a slight improvement of sensitivity while incurring a significant increase in false negative rate, i.e. a decrease in specificity.

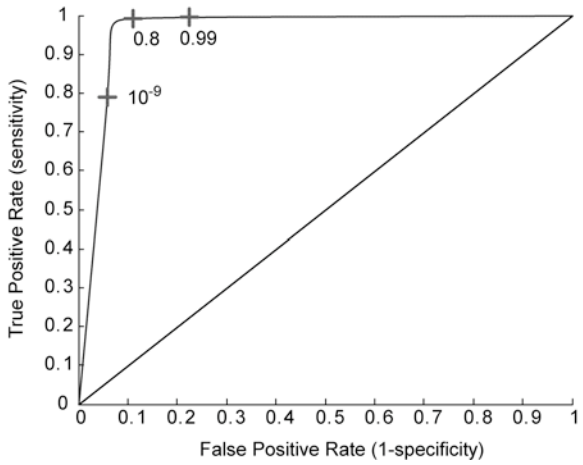

Figure 9

ROC curve of the P wave neural network classifier. The area under the curve is 0.95.

Assigning label T

The procedure for assigning label T is similar to the procedure used for P wave labeling. Since several GMFs may model a T wave, a threshold must also be chosen. A value of 0.3 results in a satisfactory tradeoff between sensitivity and specificity for T wave NNC (Figure 10). The fact that the threshold derived from the ROC curves for T waves is smaller than for P waves is due to the variability of the shape of the T wave.

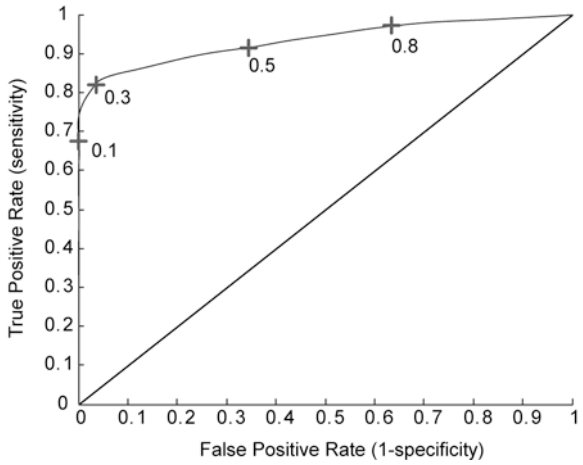

Figure 10

ROC curve of the T wave neural network classifier. The area under the curve is 0.91.

Assigning labels Q and S

Similarly, two NNCs assign labels Q and S. Label Q (resp. S) is assigned to the GMF that has the higher probability to be a Q wave (resp. S wave) if this probability is larger than 0.8.

Figure 11 summarizes the P, Q, S and T labeling process: each GMF of the model is tested for each label. A GMF that is classified as being neither R, nor P, nor Q, nor S, nor T, is assigned label X: such a GMF is considered as non-significant for the heartbeat description.

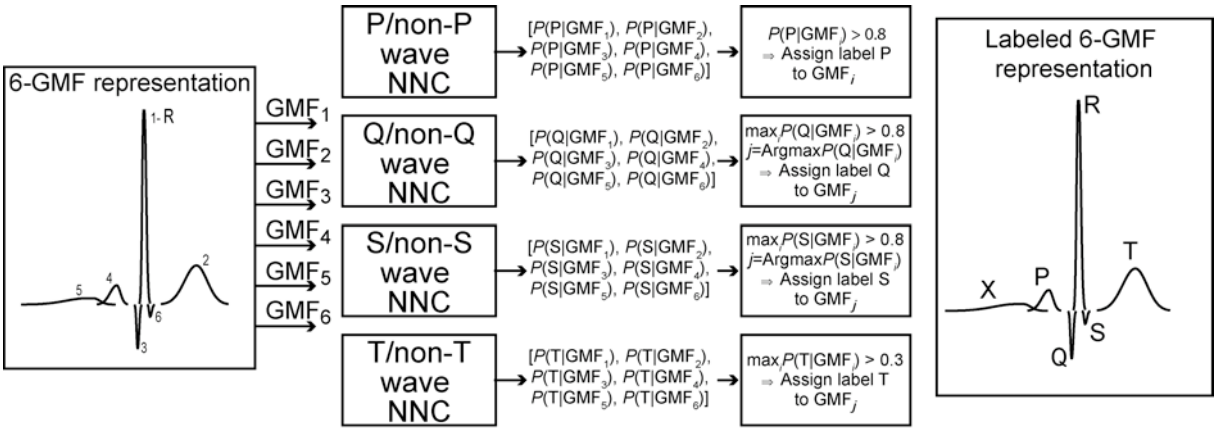

Figure 11

Global procedure for labeling the P, Q, S and T waves. The decision is made according to the label probability estimated by each NNC. GMF 5 is assigned the label X, since it is classified as being neither P, nor Q, nor R, nor S, nor T.

II.2.4. Multilead processing

The heartbeat processing (GMF decomposition and GMF labeling) described above was designed for single lead analysis. Hence, the simplest processing strategy for multilead ECG consists in processing each lead separately and subsequently making a decision as to which is the "most significant" lead for each medical label (Figure 12). One of the advantages of the GMF labeling is that the process estimates a probability for each label; these probabilities are used in the decision step to select the most significant lead for each medical label (Figure 13). For example, when processing a two-lead cardiac beat, the P wave on the first lead is modeled by one GMF out of six to which the label P is assigned with probability *P*(P-GMF*,* lead 1).

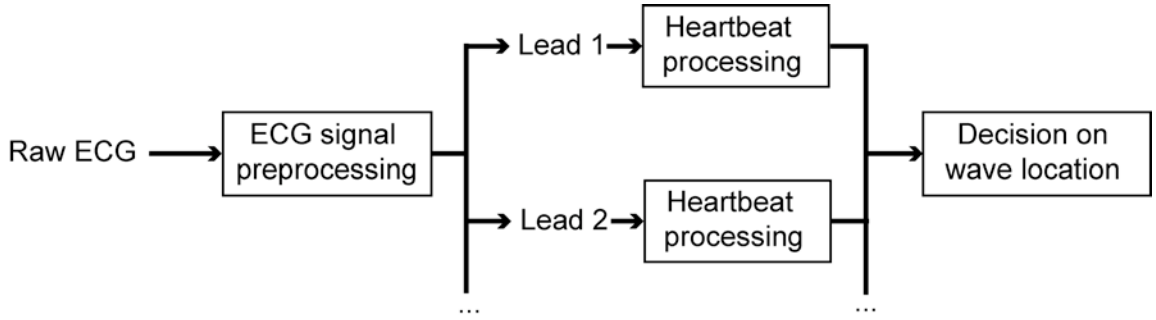

Figure 12

Global procedure for multilead analysis

Similarly, the P wave is modeled on the second lead by another GMF out of six, which is labeled P with the probability *P*(P-GMF, lead 2). The GMF selected as the most significant model of the P wave is the GMF with larger probability of being a P wave[1]: the GMF from lead 1 is chosen if *P*(P-GMF, lead 1)>*P*(P-GMF, lead 2); otherwise, the GMF from lead 2 is chosen (Figure 13).

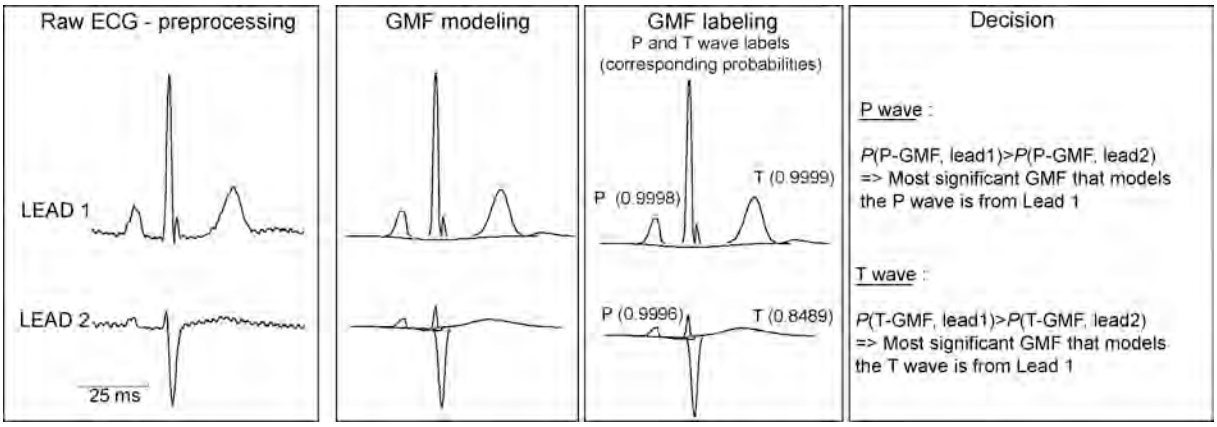

Figure 13

Example of two-lead processing: preprocessing, modelling, labelling, and decision

II.3. Post-processing

The characteristic waves of the ECG have been localized for each beat. Their shape and the distance between them are easily derived from the parameters of the corresponding GMFs.

II.3.1. Wave boundary identification

A useful feature for diagnosis is the distance between the characteristic waves, which is obtained from the position of the beginning and the end of each wave, provided by the parameters of the corresponding GMF: when a wave is modeled by a single GMF (which is by far the most frequent case in the analysis of the MIT and AHA databases), the parameters of that GMF provide information on the morphology of the wave: location of the centre, length of the linear part, half-widths of the left and right Gaussians, and amplitude (Figure 14a). The position of the centre is taken equal to μ. Since Gaussian Mesa Functions extend to infinity on either side of the maximum, the onset and offset cursors cannot be computed

[1] In the case of a biphasic wave on one of the available leads, the monophasic model of the wave, found on the other lead, is chosen as being the most significant (in standard multilead ECG recordings, at least one of the derivations will exhibit a monophasic wave).

exactly. For a Gaussian function, the beginning and the end are usually located at two standard deviations on either side of the maximum. Similarly, for Gaussian Mesa functions, the onset of the wave is defined as $\mu - 2\sigma_1 - \sigma_L/2$ and the offset as $\mu + 2\sigma_2 + \sigma_L/2$, so that the area of the GMF enclosed by the two cursors exceeds 97% of the total area; methods based on area of the T waves to exhibit the T wave offset have been shown to be efficient by other authors ([30], [31]) .

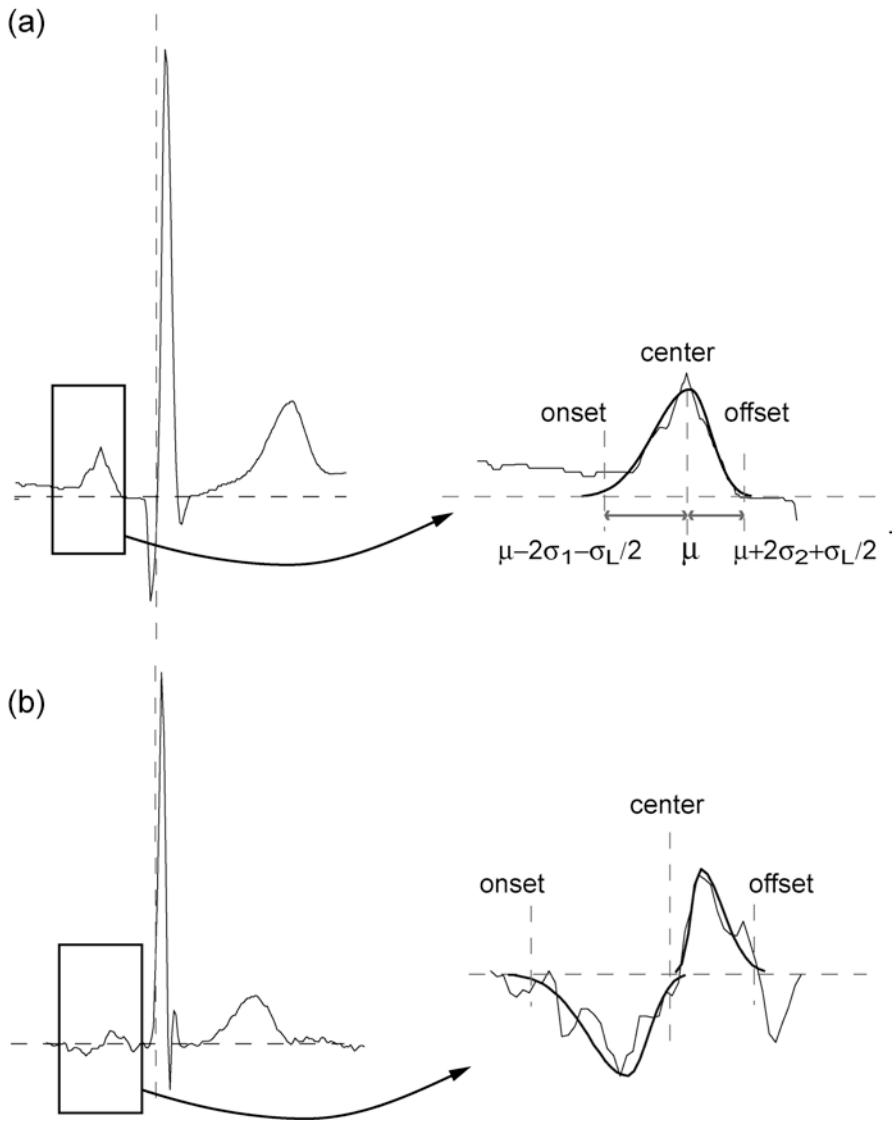

Figure 14

Wave segmentation is derived from the parameters of the GMFs. (a): in the case of a single GMF, the segmentation is derived directly from the parameters; (b) if two GMFs are required to model the wave, a decision is made from the parameters of the two GMFs, depending on their shapes.

When a biphasic P or a T wave is modeled by two GMFs, three cases may arise: (i) one GMF is wider than the other: it was found empirically that choosing the parameters of the wider GMF for segmentation provided satisfactory results; since such cases arise very infrequently in the present databases, this point will be further investigated in the future; (ii) the two GMFs overlap as illustrated on Figure 14b: the onset is taken equal to $\min\left(\mu^1 - 2\sigma_1^1 - \sigma_L^1/2,\ \mu^2 - 2\sigma_1^2 - \sigma_L^2/2\right)$, where μ^i denotes the center of GMF$_i$; the offset is taken equal to $\max\left(\mu^1 + 2\sigma_1^1 + \sigma_L^1/2,\ \mu^2 + 2\sigma_1^2 + \sigma_L^2/2\right)$; the position of the center is taken equal to $\left(\mu^1 + \mu^2\right)/2$; iii) the two GMFs do not overlap: the GMF with larger probability is used for wave delineation.

The performance of the wave boundary identification is reported in section III.

II.3.2. Amplitude, polarity and shape of the waves

The first information derived from the shape of the R wave is whether the heartbeat is normal or aberrant. When analyzing an ECG, the physician relies on expert knowledge for this discrimination: width of the R wave, R-R time interval from previous beat, R-R time interval to next beat, depolarization axis, etc. Since each R wave is modeled by a single (or two) mesa function(s), its width, its inception time, the distance to neighboring R waves, etc., are readily available. Therefore, full advantage can be taken of expert knowledge [32], [33], [34] in order to build a decision tree.

A time change in the cardiac wave shapes is an additional useful feature for the experts to perform a diagnosis. Figure 15 shows an episode of abnormal atrial activity on a 24-hour ECG: the P waves are upside down from the sixth beat onward. The detection of such activity is very difficult from rhythm analysis, because of the stability of the R-R intervals. Our methodology localizes the P waves for each beat, and models it with a GMF, so that the amplitude of the P wave for each beat is known. In order to detect this pathology automatically, the amplitude of the GMF that modeled the P wave can be plotted as a function of time (Figure 16): the GMF amplitude is negative for these ectopic beats. Note that the latter curve is already available to cardiologist on short-term ECG for patients in supine position, but has never been presented on long-term ambulatory ECG analysis.

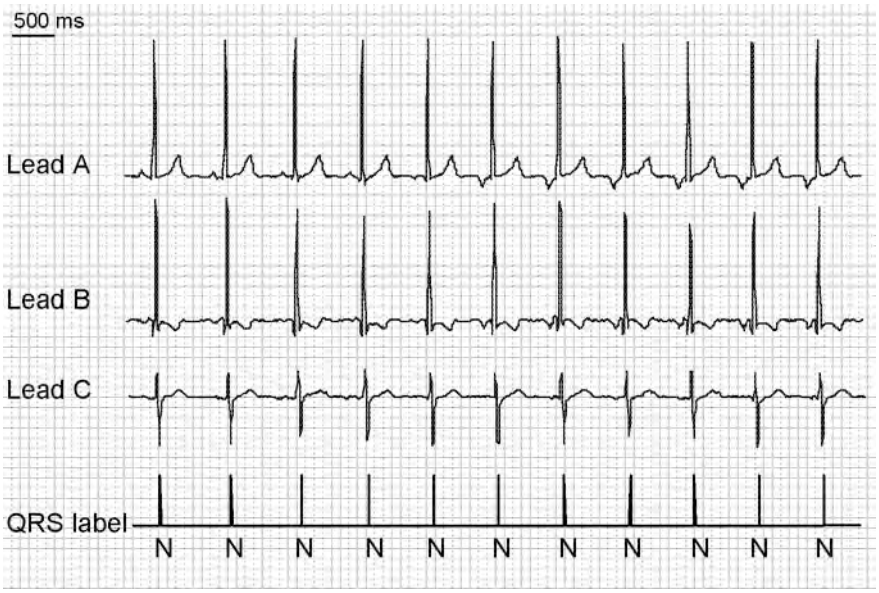

Figure 15

ECG with an abnormal atrial activity. From the sixth beat onward, the P wave is upside down. The rhythm is still very stable during the occurrence of this conduction anomaly; therefore, it is very hard to detect from rhythm analysis.

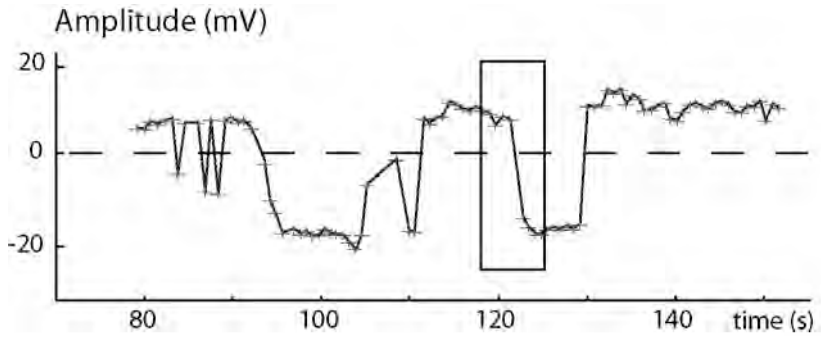

Figure 16

Time evolution of the amplitude of the P wave (mV). The rectangle contains the part of the recording that is displayed on Figure 15 . Each cross is a heartbeat. The abnormal atrial activity appears clearly in this representation.

Figure 17 shows a two-lead ECG from the MIT database (record 119), labeled by our algorithm. In this figure, only the beginning of the P and the end of the T waves are labeled for each beat. These results are obtained without any expert annotation. The abnormal beats have been detected by the discrimination step described above. But the abnormality appears also on other features extracted by the algorithm.

Figure 17

Automatic annotation of ECG with the present algorithm. The GMF decomposition of the cardiac beats marked by an asterisk is shown on Figure 19.

For example, Figure 18 shows the evolution in time of the T wave amplitude on lead A; the upside-down repolarisation of the abnormal beats appears clearly on this graph. Figure 19 shows the GMF decomposition of two consecutive beats (one normal and one abnormal). The GMF labelling process did not assign label "P" to any wave of the abnormal beat; this absence can also be a flag for abnormality.

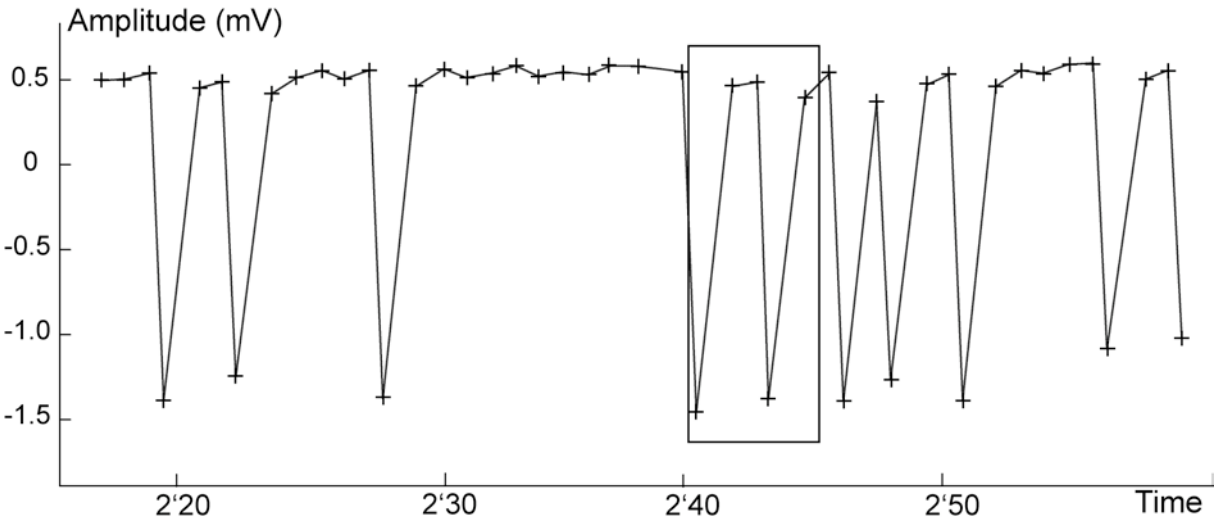

Figure 18

Evolution in time of the T wave amplitude. The rectangle contains the part of the recording that is displayed on Figure 17. The variation of repolarisation direction is a flag of abnormality.

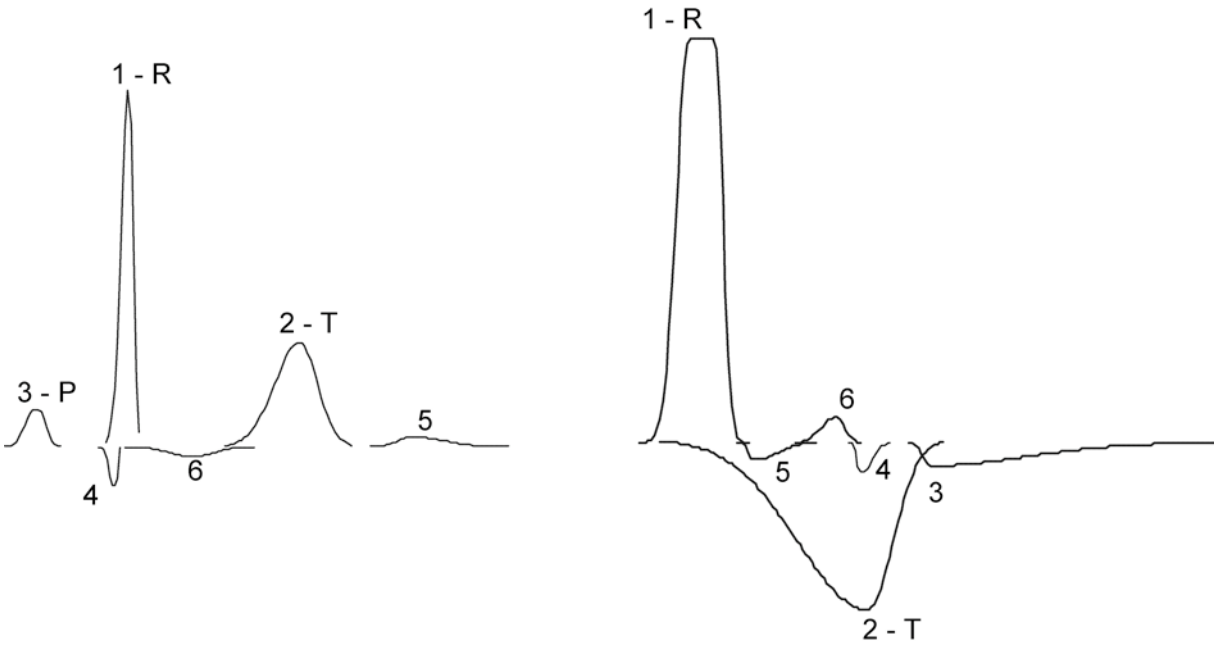

Figure 19

GMF decomposition and labelling of two consecutive beats marked by asterisks on Figure 17. The absence of label P in the second decomposition is a flag for abnormality

II.4. Implementation and computation time

The procedure has been developed under the Matlab environment. The optimisation step with GOFR is in C-code to increase speed. At present, 36 ms are required to model and label 100 heartbeats[2]; therefore, brute-force GMF modeling of the 180,000 heartbeats of a 24-hour recording would require more than one minute. For routine use, this is too long because the global analysis procedure requires additional time-consuming steps such as QRS detection, baseline cancellation and wave labeling, while an automatic analysis of long term ECG (Holter record) must be performed within a few minutes. To shorten the modeling step, similar heartbeats were grouped together by an unsupervised clustering procedure (see [26] for details) based on several features of the heartbeat (RR interval from previous beat, RR interval to next beat, QRS principal axis direction, shape of the QRS loop). That step resulted in less than 200 clusters for the 180,000 heartbeats, which reduces the expected computation time for the global analysis procedure to about 2 minutes for a 24-hour recording.

In its final version, the whole procedure will be implemented in the ELA Medical Holter analysis software for clinical use.

---

[2] C program running under Windows XP on a Pentium IV-m, 2.8 Ghz

III. Results

This section describes the results of the global procedure (Figure 1). The results pertaining to heartbeat recognition (NB vs AB) are first described; results for P and T wave localization are presented in the second subsection. All results reported below were obtained on test sets, i.e. on heartbeats that were used neither for training nor for optimizing the NNC classifiers.

III.1. Cardiac beat recognition: NB vs. AB

The performance of the discrimination of normal beats from abnormal beats was estimated on the MIT database[3] [23], and the AHA database[4] [22]. In this paper, we considered as abnormal beats, beats which did not come from AV node. Beats labeled in the MIT database as normal, atrial premature beat, nodal premature escape beat, or bumble branch beat are considered as normal beat in this study, and beats labeled as ventricular contraction are considered as abnormal. Beats labeled as fusion beats that correspond to a depolarization from ventricular and from AV node merged together were not taken into account for performance estimation.

The sensitivity (S) and the positive predictivity (P_+) are reported in Table 2:
$S = T_P / (T_P+F_N)$ and $P_+ = T_P / (T_P+F_P)$
where T_P is the number of true positive detections, and F_N (resp. F_P) is the number of false negatives (resp. false positives).
These results involve both heartbeat localization and recognition. Thus, the value of S for normal beats, for example, reflects the efficiency of the algorithm for detecting the QRS location *and* labeling it as a normal beat. These results are better than, or in the same range as, results obtained by state-of-the-art published methods (e.g. [11], [12] ,[35], [36]), and they provide a substantial improvement over results obtained by commercially available programs on the same databases [12].

[3] We discard records #102, #104, #107, and #217 in the MIT database as they correspond to pacemaker records.

[4] We discard series 800x in the AHA database. These records are ventricular fibrillation, so that the ventricle depolarization in not well defined in such cases.

		MIT Database		AHA Database	
		Normal beats	Abnormal beats	Normal beats	Abnormal beats
Present algorithm	Number of analyzed beats	86,071	4,771	131,949	11,407
	Sensitivity *S* (%)	99.80	91.72	99.68	87.77
	Positive predictivity *P*+ (%)	99.47	95.46	98.95	95.93
Coast et al [36]	Number of analyzed beats	N/S	N/S	14,350	799
	Sensitivity *S* (%)	N/S	N/S	99.82	97.25
	Positive predictivity *P*+ (%)	N/S	N/S	98.90	85.67
Martinez et al [12] *	Number of analyzed beats	109,428		N/S	N/S
	Sensitivity *S* (%)	99.80		N/S	N/S
	Positive predictivity *P*+ (%)	99.86		N/S	N/S
Pan et al [24] *	Number of analyzed beats	109,809		N/S	N/S
	Sensitivity *S* (%)	99.75		N/S	N/S
	Positive predictivity *P*+ (%)	99.54		N/S	N/S

Table 2

Results for R wave assignment and heartbeat labeling on MIT[3] and AHA[4] databases.

*** Values that refer to QRS detection only without normal/abnormal beats discrimination**

III.2. P and T labeling on QTDB database

In the present section, the neural network classifiers trained on the ELA medical database (as described in section II) were applied, without further processing, to the labeling of P and T waves present in the records of the QTDB database [35]. To the best of our knowledge, only two public databases contain manually annotated P, R and T waves: the QTDB database, and the CSE database [37]. The characteristics of the QTDB database (signal length, number and position of the leads, sampling rates) are much closer to those available with Holter records than the CSE database. Table 3 (from {Schreier, 2003}) summarizes the differences between the QTDB and CSE databases.

QTDB features a significant number of records, sampled from well-known databases such as MIT database or AHA database, and manually annotated by an expert. It includes 3,622 annotated beats, with a variety of ECG morphologies (3,194 P waves and 3,542 T waves).

Moreover, QTDB is known to have a very poor signal to noise ratio, with several pathologies that make an accurate detection of the waves over the whole database a challenging task. Therefore, at present, QTDB is the only annotated database that is relevant for testing our method for analyzing long-term recordings.

Property	QTDB (PhysioNet)	CSE Multilead
Signal length	About 15 min	About 10 s
Sample rate	250 Hz	500 Hz
Number of channels	2	15 (12 standard leads and 3 orthogonal leads)
Number of signals containing markers for QRS onset et T offset	103	25
Number of annotated beats per signal	30 to 80	1
Total number of annotated events	3623 (QRS onset), 3542 (T offset)	25 (QRSonset), 25 (T offset)
Location of experts' annotations within signal	About 10min after the beginning of the signal	First beat only
Number of experts	One, except for 11 signals with two experts	5

Table 3

Comparison of QTDB and CSE databases (from table 1 of {Schreier, 2003}).

III.2.1. Single lead processing

The first two rows of Table 4 contain the results for lead 1 and lead 2 when each lead is processed separately. The third row shows the results obtained when the marker from the two leads that agreed most with the annotation was selected. The latter methodology was described in [12].

	Markers	P_{on}	P_{peak}	P_{end}	T_{peak}	T_{end}
	# of annotations	3,194	3,194	3,194	3,542	3,542
Present algorithm Lead 1	S (%)	80.9	80.9	80.9	82.1	82.1
	E (ms)	22.6	15.5	21.1	29.2	45.0
	σ (ms)	22.6	12.2	22.3	17.9	38.6
Present algorithm Lead 2	S (%)	76.2	76.2	76.2	81.6	81.6
	E (ms)	24.7	18.1	27.2	25.4	42.8
	σ (ms)	25.7	16.3	31.2	17.4	40.3
Present algorithm Best lead	S (%)	91.2	91.2	91.2	93.6	93.6
	E (ms)	17.3	11.1	17.6	19.9	34.8
	σ (ms)	17.7	8.9	18.6	12.0	30.3
Ref1 vs ref2	E_{ref} (ms)	-	-	-	17.5	24.5

Table 4

Results for P and T labeling on the QTDB database for single lead processing. P waves are described by P_{on}, P_{peak} and P_{end} markers; for T waves, T_{peak} and T_{end} only are annotated.

To estimate the performance, three values are shown: first, the sensitivity of the algorithm for each marker; second, the mean magnitude of the error E over all annotated beats:

$$E = 1/N \sum_{i=1..N} \left| m^i_{ann} - m^i_{alg} \right| \quad (1)$$

where N is the number of detected markers of a given type, m^i_{ann} the position in time of the i-th annotator's marker, and m^i_{alg} the position found by our method. Therefore, E=0 if all markers from the algorithm are exactly at the same positions as the markers of the annotator.

Some publications ([12], [35]) define the error as the algebraic value of the discrepancy between the position of the annotator's marker and the position of the computed marker, rather than the absolute value of that discrepancy. In those papers, the results are given in terms of mean value of this algebraic discrepancy and its standard deviation. To compare our results with those publications, the third value given in Table 4 is the value of the error (σ) such that Pr($E < \sigma$) = 0.67. This value can be directly compared to the standard deviation (*Std*) of publications that use algebraic values of the error.

For 11 records of the QTDB database, a second reference for T waves is available from a second cardiologist ("second annotator"); the last row of the table provides the difference between the two annotations (the first annotation was used as a reference; E_{ref} is the mean magnitude of the difference between the two annotations, for each marker): these values can be viewed as the maximum performance that one can expect from automatic detection, assuming that humans cannot be outperformed for annotation.

The distribution of the magnitude of the error for the P wave is shown on Figure 20. For the onset marker and the offset marker, the results obtained for that wave are in the same range as those published previously (for a review see [12], table III). The marker that labels the peak of the P wave is more accurate with the methodology described here, but the sensitivity is slightly lower[5].

5 The distributions displayed on Figure 20 and Figure 22 are those obtained when the marker that best agrees with the annotation is selected.

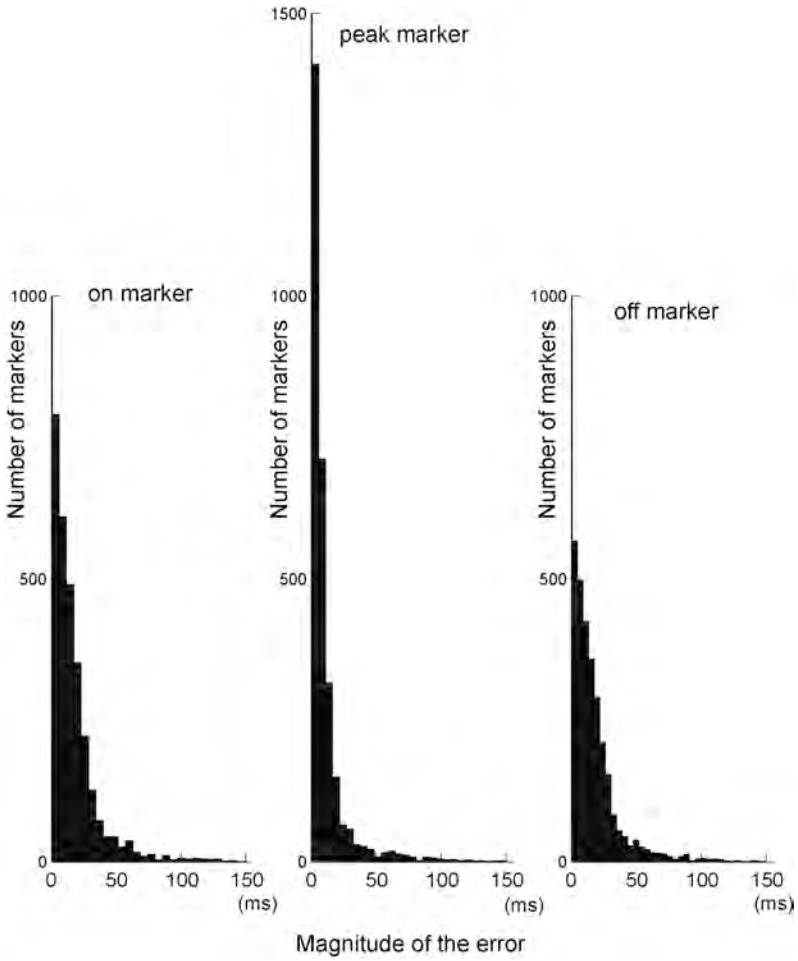

Figure 20

Distribution of the magnitude of the error for P wave markers

Some automatically detected markers have a large discrepancy with the annotators' markers, so that they contribute heavily to the overall error. One example of such cases is shown on Figure 21: the P wave has the same amplitude as noise, which makes its automatic detection very difficult.

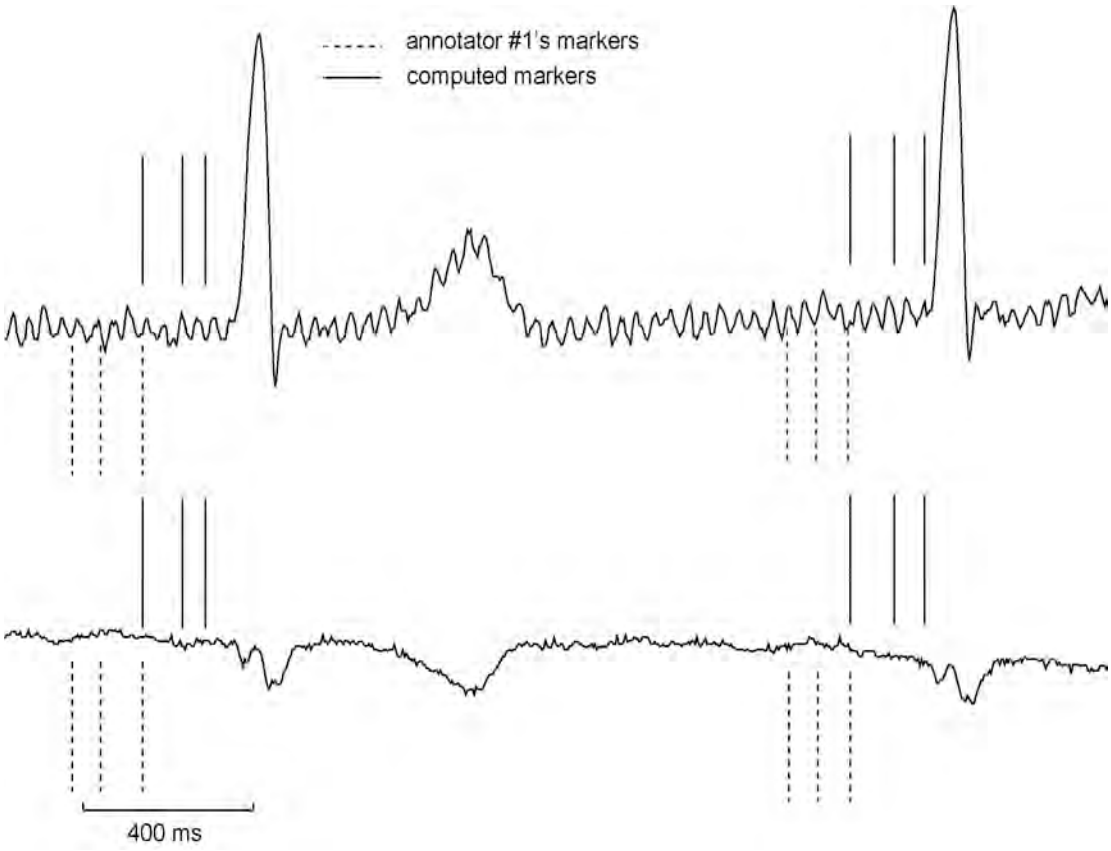

Figure 21

Record (sele0116, 0:10:17.5): the P wave has a low signal-to-noise ratio; the differences between the annotator's marker and the computed marker for the first beat are 156ms, 185ms, 140ms for the on, peak and off markers respectively; such values give large contributions to the overall error.

The results for T wave location are less accurate than those obtained for the P wave. Nevertheless, these results are better than those published in [8]. They are in the same range as those published in [10], [12] for the peak of the wave, and slightly lower for the end of the wave. However, the quality of the T wave markers appears clearly when comparing the results to the annotator's error E_{ref}: the difference between the two errors (E_{ref} and E) on both T wave peak marker and T wave offset marker is less than 2 samples (~8 ms, since QTDB is sampled at 250Hz).

Distributions of the error on the T wave markers are shown on Figure 22. Just as for the P wave marker histograms, a few large values of some errors have large adverse effects on the average results. One example of record with large errors is shown on Figure 23: in this case, the T wave is bifid. The annotator's markers include only the first part of the T wave whereas the present algorithm markers include the two parts of the wave. The peak of the wave is between the two parts of the wave as described in section II.3.1. Thus, the comparison between markers on such heartbeats produces large discrepancies.

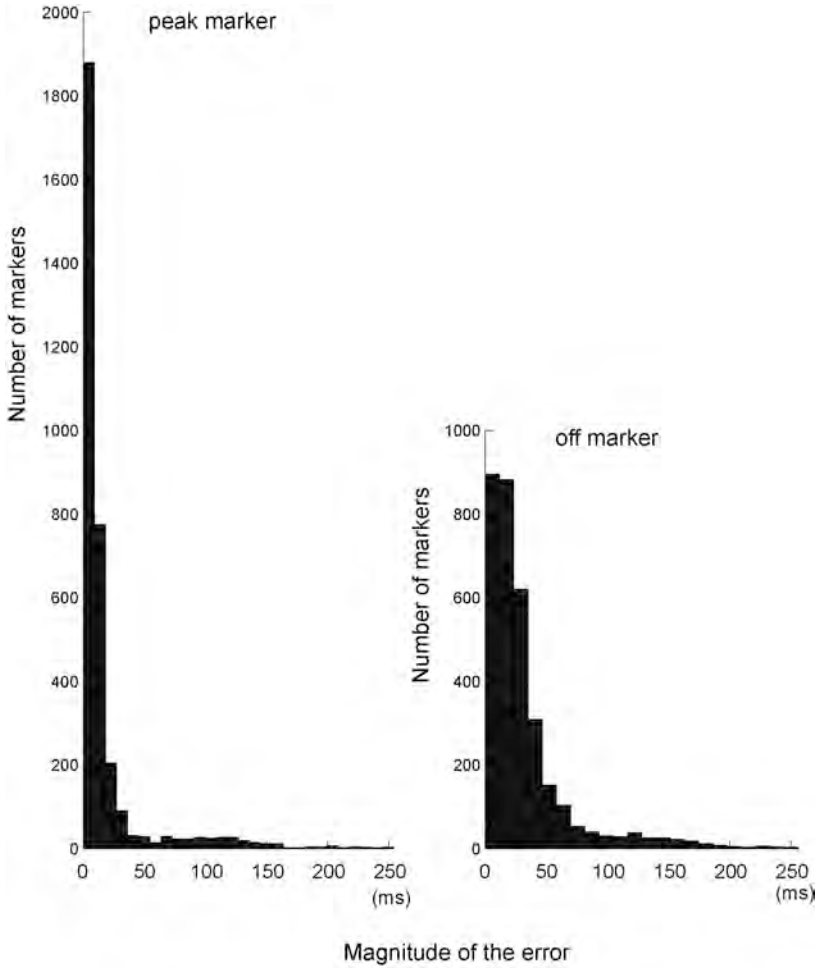

Figure 22

Distribution of the magnitude of the error for T wave markers

III.2.2. Multilead processing

As indicated in section II.2.4, three markers for the P waves (onset, peak and offset) and two markers for the T wave (peak and offset) are provided for each cardiac beat from the multilead processing; these markers take into account the information from all available leads.

Table 5 shows the results obtained on QTDB. Similarly to single lead processing, the performances of the algorithm are measured by the magnitude of the discrepancy between each annotator marker and the corresponding computed marker.

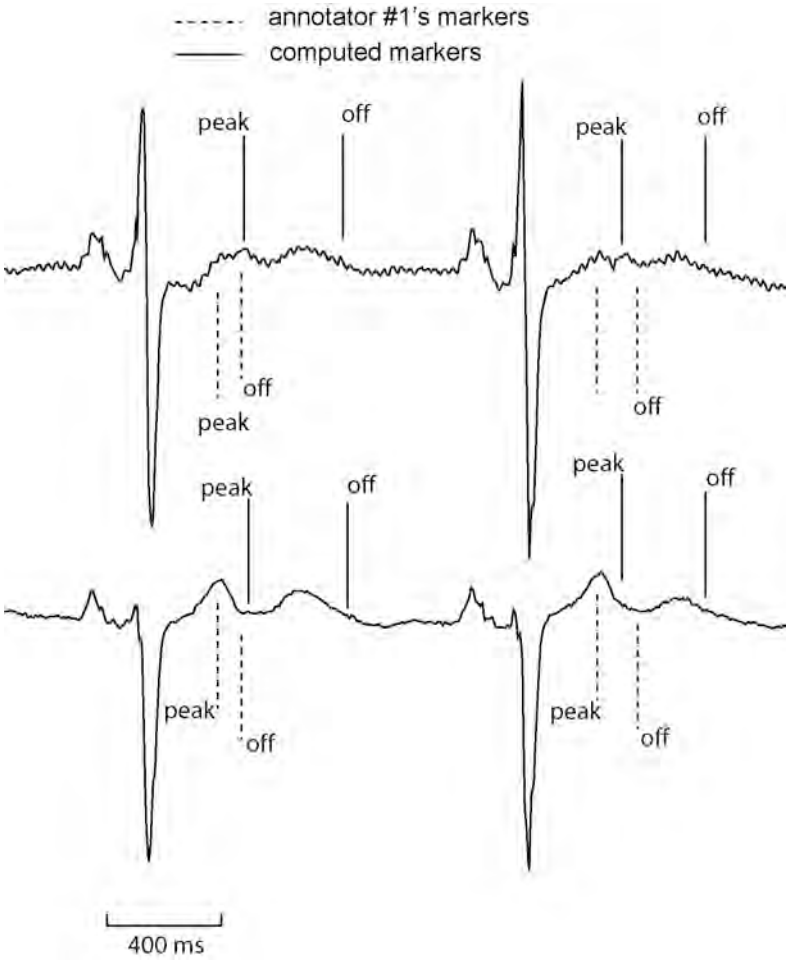

Figure 23

In this record (sel14172, 10:17:20) the T wave is bifid. For both heartbeats, the GMF decomposition models the T wave with 2 GMFs and the neural network classifier detects the more accurate T-GMFs on lead II.

	Parameters	Pon	Ppeak	Pend	Tpeak	Tend
	# of annotations	3,194	3,194	3,194	3,542	3,542
Presented algorithm	E (ms)	19.6	14.3	20.6	26.9	42.8
Multilead processing	σ (ms)	20.0	12.2	21.4	18.4	38.5
Ref1 vs ref2	Eref (ms)	-	-	-	17.5	24.5

Table 5

Result of P and T labeling on the QTDB database for multilead processing. P waves are described by P_{on}, P_{peak} and P_{end} markers; for T waves, T_{peak} and T_{end} only are annotated.

The results for multilead processing are less accurate than those obtained for single lead processing when the best lead is selected for each marker, but are much better than those obtained from a single lead when only one lead is processed. The magnitude of the error on the P wave detection is approximately 5 sampling periods for the onset and end markers, and

smaller than 4 sampling periods for its peaks; 67% of the markers have an error in those ranges. Similar to single lead processing, a few markers give a large contribution to the overall error: distributions are shown for each marker on Figure 24.

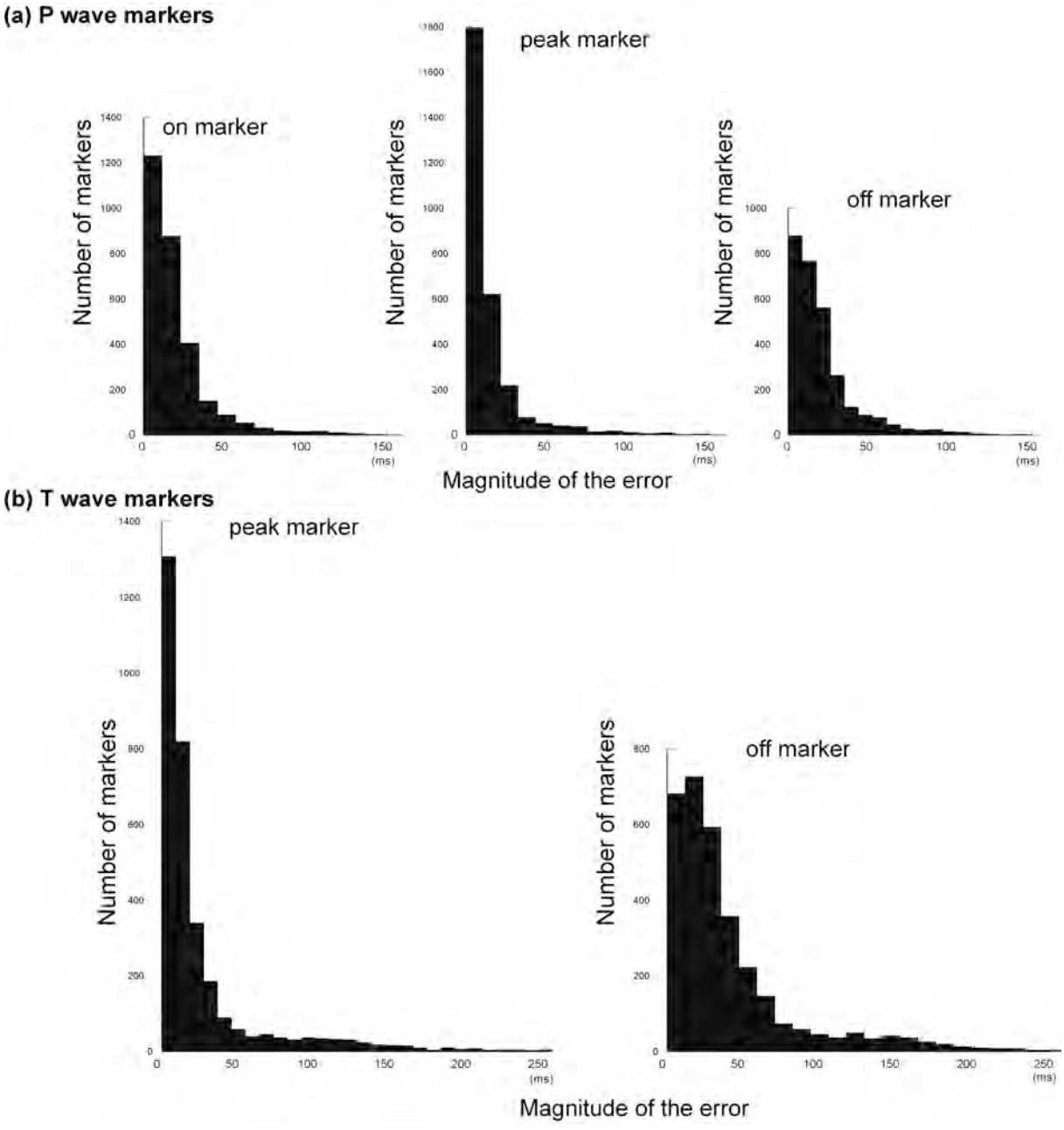

Figure 24

Distribution of each marker for the P wave (a) and for the T wave (b)

The peak of the T wave is detected with an error below 6 sampling periods, and below 9 sampling periods for its end. However, 67% of the markers have an error smaller than 5 sampling periods for the peak of the wave.

These results are slightly less accurate than those published in [8], [12], but these studies refer to single lead processing, and the best marker from available leads is chosen to compute the error. Here, the processing includes multilead decision, which is a more realistic configuration in the framework of automatic processing.

IV. Conclusion and discussion

The present paper described an algorithm for labeling automatically the characteristic waves of an ECG. We first described a methodology for representing the heartbeat as a combination of special-purpose parameterized functions (GMFs) in order to extract discriminant features. We also discussed the design of nonlinear classifiers for assigning automatically a medical label (P, Q, R, S and T) to each GMF of the model.

Heartbeat modeling and labeling is a part of a global procedure that processes raw data from multilead records, without any pre-processing by the cardiologist: it detects R waves, removes the baseline and labels the waves. It was tested on the MIT and AHA databases for R wave localization, and on QTDB for P and T wave detection. The results are very satisfactory, especially for multilead processing. At present, wave delineation is performed from the GMF parameters with very simple rules; that part of the algorithm can probably be improved in order to decrease the magnitude of the error of the marker. Moreover, in the present method, multilead processing is performed by choosing, for each beat, the lead from which wave delineation is statistically most probable (based on GMF probability), so that the final wave delineation is made from a single lead. Two strategies emerge to improve the results: first, in order to take advantage of all available information, all GMFs that are assigned the same label could be taken into account, e.g. for wave delineation; alternatively, principal component analysis (PCA) could be performed on each heartbeat in order to find the most informative direction [26], [38], [39], [40]. GMF modeling and labeling of the principal component (or possibly of the two principal components) should improve the robustness of the computation.

In addition to their use for wave delineation, GMFs provide five parameters that describe the shape of each wave. This property is a powerful tool for temporal detection of shape changes in specific characteristic waves, and provides the expert with new diagnosis tools on the whole ambulatory long-term ECG.

Finally, it should be noted that a significant part of the methodology described here is generic, and can be applied outside the field of cardiology. An extension to 2-dimensional signals (time-frequency maps) has been performed, and applied to the analysis of neurophysiological, e.g. for the early detection of Alzheimer's disease [41], [42].

Acknowledgements

The authors are grateful to S. Christophle-Boulard and Dr Y. Faisandier for discussions; they wish to thank A. Rippart for supporting this work.

Appendix A

Given an unknown pattern described by a vector of numbers ("features"), a single-output neural network classifier (NNC) is a parameterized function that provides an estimate of the posterior probability of the classes, i.e. the probability that the pattern belongs to one of two classes (posterior probability) (Figure 25).

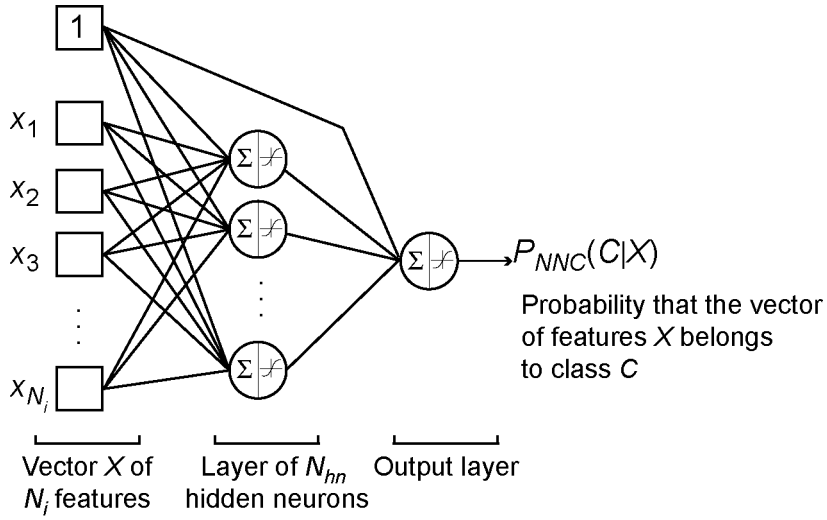

Figure 25

Neural network classifier

The features are fed to an appropriate number of elementary functions ("hidden neurons") each of which computes a nonlinear function (tanh) of a weighted sum of the features. The "output neuron" computes a nonlinear function (logistic function) of the quantities computed by the "hidden" neurons. The weights of the weighted sums are the parameters of the model (2).

$$P_{NNC}\left(C\middle|X\right)= f\left(\sum_{i=1..N_{hn}} \theta_i^{out} \tanh\left(\sum_{j=1..N_i} \theta_{ij}^{in} x_j + \theta_{i0}^{in}\right) + \theta_0^{out}\right) \qquad \textbf{(2)}$$

where P_{NNC} is the output of the NNC, $X = \begin{bmatrix} x_1 & x_2 & \cdots & x_{N_i} \end{bmatrix}^T$ is the feature vector, and N_{hn} is the number of hidden neurons. f is the logistic function. The parameters of the network are:

- $\left\{\theta_i^{out}\right\}_{i=1..N_{hn}}$, pertaining to the "connections" between the N_{hn} hidden neurons (i = 1 to N_{hn}) and the output neuron;

- $\left\{\theta_{ij}^{in}\right\}_{j=1..N_i}$, pertaining to the connections between the N_i features (j = 1 to N_i) and hidden neuron i,
- $\left\{\theta_{i0}^{in}\right\}_{i=1..N_{hn}}$, pertaining to the connections between the constant input (equal to 1, called *bias*) and hidden neuron i
- θ_0^{out}, pertaining to the connection between the bias and the output neuron.

These parameters are estimated through an algorithmic process ("training"), from a set of examples of the patterns to be classified ("training set"), by minimizing a cost function J. In the present case, the least squares cost function was minimized:

$$J(\boldsymbol{\theta}) = \frac{1}{N_p} \sum_{k=1..N_p} \left(L(k) - P_{NNC}\left(C \middle| X_k\right)\right)^2 \quad \textbf{(3)}$$

where N_p is the size of the training set, $L(k)$ = 1 if input vector X_k belongs to class C and $L(k)$ = 0 otherwise.

For classification problems, alternative cost functions can be used such as cross entropy; interested readers can refer to [43],[44].

The complexity of the classifier is determined by the number of hidden neurons; a neural network with zero hidden neuron is a linear separator: the locus of points of equal probability is a straight line. The larger the number of hidden neurons, the more complex the separation between classes of examples that is performed by the classifier. If the network is too complex, the classifier is too sensitive to the details of the training set and gives poor results when presented with fresh data; conversely, if the classifier is not complex enough, it is unable to classify the examples of the training set (the so-called "bias-variance dilemma"). Therefore, model selection is an important part of the model design process ([43], [44] ,).

Alternative statistical classifiers, such as support vector machines [45], could be used in the same context. However, given the small dimensionality of input space, and the large number of available examples, neural networks are appropriate for the present task. In addition, support vector machines are not well suited to probability estimation, which is of central importance in our procedure.

References

[1] G.S. Wagner, H.J.L. Marriott, Marriott's practical electrocardiography, (Lippincott Williams & Wilkins, 2001, Philadelphia).

[2] M.H. Crawford, S.J. Bernstein, P.C. Deedwania, J.P. DiMarco, K.J. Ferrick, A. Garson, Jr., L.A. Green, H.L. Greene, M.J. Silka, P.H. Stone, C.M. Tracy, R.J. Gibbons, J.S. Alpert, K.A. Eagle, T.J. Gardner, G. Gregoratos, R.O. Russell, T.J. Ryan, S.C. Smith, Jr., ACC/AHA guidelines for ambulatory electrocardiography: executive summary and recommendations. A report of the American College of Cardiology/American Heart Association task force on practice guidelines (committee to revise the guidelines for ambulatory electrocardiography). Circulation, (1999), 100, 886-93.

[3] P.R. Kowey, D.Z. Kocovic, Cardiology patient pages. Ambulatory electrocardiographic recording. Circulation, (2003), 108, e31-3.

[4] P. Laguna, G.B. Moody, J. Garcia, A.L. Goldberger, R.G. Mark, Analysis of the ST-T complex of the electrocardiogram using the Karhunen--Loeve transform: adaptive monitoring and alternans detection. Med Biol Eng Comput, (1999), 37, 175-89.

[5] E. Soria-Olivas, M. Martinez-Sober, J. Calpe-Maravilla, J.F. Guerrero-Martinez, J. Chorro-Gasco, J. Espi-Lopez, Application of adaptive signal processing for determining the limits of P and T waves in an ECG. IEEE Trans Biomed Eng, (1998), 45, 1077-80.

[6] Y. Sun, K.L. Chan, S.M. Krishnan, Characteristic wave detection in ECG signal using morphological transform. BMC Cardiovasc Disord, (2005), 5, 28.

[7] F. Gritzali, G. Frangakis, G. Papakonstantinou, Detection of the P and T waves in an ECG. Comput Biomed Res, (1989), 22, 83-91.

[8] J.A. Vila, Y. Gang, J.M. Rodriguez Presedo, M. Fernandez-Delgado, S. Barro, M. Malik, A new approach for TU complex characterization. IEEE Trans Biomed Eng, (2000), 47, 764-72.

[9] K. Sternickel, Automatic pattern recognition in ECG time series. Comput Methods Programs Biomed, (2002), 68, 109-15.

[10] P. Laguna, R. Jane, P. Caminal, Automatic detection of wave boundaries in multilead ECG signals: validation with the CSE database. Comput Biomed Res, (1994), 27, 45-60.

[11] C. Li, C. Zheng, C. Tai, Detection of ECG characteristic points using wavelet transforms. IEEE Trans Biomed Eng, (1995), 42, 21-8.

[12] J. Martinez, R. Almeida, S. Olmos, A. Rocha, P. Laguna, A wavelet-based ECG delineator: evaluation on standard databases. IEEE Trans Biomed Eng, (2004), 51, 570-81.

[13] S. Suppappola, Y. Sun, S.A. Chiaramida, Gaussian Pulse Decomposition: An intuitive Model of Electrocardiogram Waveforms. Annals of Biomedical Engineering, (1997), 25, 252-60.

[14] B.P. Simon, C. Eswaran, An ECG classifier designed using modified decision based neural networks. Computer and Biomedical Research, (1997), 30, 257-72.

[15] S. Osowski, T. Linh, ECG beat recognition using fuzzy hybrid neural network. IEEE Trans Biomed Eng, (2001), 48, 1265-71.

[16] A. Koski, Modelling ECG Signals with Hidden Markov Models. Artificial Intelligence in Medicine, (1996), 8, 453-71.

[17] L. Thoraval, G. Carrault, J.J. Bellanger, Heart Signal Recognition by Hidden Markov Models: The ECG Case. Methods of Information in Medicine, (1994), 33, 10-14.

[18] L. Senhadji, L. Thoraval, G. Carrault, Continuous wavelet transform: ECG recognition based on phase and modulus representations and hidden Markov model. Wavelet Applications in Medicine and Biology, (1996), 439-63.

[19] S. Jankowski, J. Tijink, G. Vumbaca, B. Marco, G. Karpinski, 2002. Morphological Analysis of ECG Holter Recordings by Support Vector Machines. In: Proceedings of the Third International Symposium on Medical Data Analysis, Springer-Verlag,

[20] K. Poon, P.M. Okin, P. Kligfield, Diagnostic performance of a computer-based ECG rhythm algorithm. J Electrocardiol, (2005), 38, 235-8.

[21] S.M. Salerno, P.C. Alguire, H.S. Waxman, Training and competency evaluation for interpretation of 12-lead electrocardiograms: recommendations from the American College of Physicians. Ann Intern Med, (2003), 138, 747-50.

[22] AHA-DB, AHA Database Series 1, (The American Heart Association Electrocardiographic - ECRI, 1997).

[23] MIT-DB, The MIT-BIH Arrhythmia database (third edition), (Massachusetts Institute of Technology - http://ecg.mit.edu, 1997).

[24] J. Pan, W.J. Tompkins, A real-time QRS detection algorithm. IEEE Trans Biomed Eng, (1985), 32, 230-6.

[25] J. Stephenson, 2000. Detection of Isoelectric Baseline and High Frequency Noise within Electrocardiographique Signal. In: ESPCI, Laboratoire d'Electronique - http://www.neurones.espci.fr/Francais.Docs/STEPHENSON.htm,

[26] R. Dubois, (2003). Application des nouvelles méthodes d'apprentissage à la détection précoce d'anomalie en électrocardiographie. PhD thesis in: Laboratoire d'Electronique, ESPCI, Paris-France.

[27] R. Dubois, B. Quenet, Y. Faisandier, G. Dreyfus, Building meaningful representations for nonlinear modeling of 1d- and 2d-signals: applications to biomedical signals. Neurocomputing, (2006), 69, 2180-92.

[28] C.G. Broyden, The Convergence Double Rank Minimization Algorithms. 2. The New Algorithm. J. Inst. Maths Applics, (1970), 6, 222-31.

[29] C.E. Metz, Basic Principles of Roc Analysis. Seminars in Nuclear Medicine, (1978), 8, 283-98.

[30] Q. Xue, S. Reddy, Algorithms for computerized QT analysis. J Electrocardiol, (1998), 30 Suppl, 181-6.

[31] J.P. Couderc, W. Zareba, A.J. Moss, N. Sarapa, J. Morganroth, B. Darpo, Identification of sotalol-induced changes in repolarization with T wave area-based repolarization duration parameters. J Electrocardiol, (2003), 36 Suppl, 115-20.

[32] N. Holter, New method for heart Studies. Science, (1961), 134, 1214-29.

[33] P. MacFarlane, L. Veitsch, Comprehensive Electrocardiology: Theory and Pratice in Health and disease, (Pergamon Press Inc, 1989, New York).

[34] J.W. Hurst, Ventricular Electrocadiography, (Lippincot Williams & Milkins Publishers, 1990).

[35] P. Laguna, R. Mark, A. Goldberger, G. Moody, A Database for Evaluation of Algorithms for Measurement of QT and Other Waveform Intervals in the ECG. Computers in cardiology, (1997).

[36] D.A. Coast, G.G. Cano, S.A. Briller, Use of Hidden Markov Model for Electrocardiographic Signal Analysis. Journal of Electrocardiology, (1991), 23 suppl, 184-91.

[37] Recommendations for measurement standards in quantitative electrocardiography, The CSE Working Party. Eur Heart J, (1985), 6, 815-25.

[38] R. Lux, Principal Components Analysis: An Old but Powerful Toll for ECG Analysis. International Journal of Bioelectromagnetism, (2003), 5, 342-45.

[39] S. Leanderson, P. Laguna, L. Sörnmo, Estimation of the Respiratory Frequency using Spatial Information in the VCG. Med Eng Phys, (2003), 25, 501-07.

[40] J. Berg, J. Fayn, L. Edenbrandt, B. Lundh, P. Malmstrom, P. Rubel, CAVIAR: a tool to improve serial analysis of the 12-lead electrocardiogram. Clin Physiol, (1995), 15, 435-45.

[41] F. Vialatte, G. Chichocki, G. Dreyfus, T. Musha, M. Rutkowski, R. Gervais, Blind Source Separation and Sparse Bump Modeling of Time-Frequency Representation of EEG Signals: New Tools for Early Detection of Alzheimer's Disease. Machine Learning for Signal Processing (MLSP 2005), (2005).

[42] F.B. Vialatte, C. Martin, R. Dubois, J. Haddad, B. Quenet, R. Gervais, G. Dreyfus, A machine learning approach to the analysis of time-frequency maps, and its application to neural dynamics. Neural Networks, (2007), 20, 194-209.

[43] C. Bishop, Neural Networks for pattern recognition, (Clarendon Press - Oxford, 1995).

[44] G. Dreyfus, Neural Networks, Methodology and Applications, (Springer, 2005).

[45] N. Cristianini, J. Shawe-Taylor, An Intoduction to Support Vector Machines, (University Press, 2000, Cambridge).